



Effects of radiation on mixed convection stagnation-point flow of MHD third-grade nanofluid over a vertical stretching sheet

Bijan Golafshan¹ · Asghar B. Rahimi¹

Received: 24 January 2018 / Accepted: 10 February 2018 / Published online: 22 February 2018
© Akadémiai Kiadó, Budapest, Hungary 2018

Abstract

This paper considers the problem of the two-dimensional mixed convection stagnation-point flow of a magnetohydrodynamic non-Newtonian nanofluid bounded by a vertical stretching sheet. Convective surface boundary and zero surface nanoparticle mass flux conditions are employed. The effects of buoyancy, radiation, Brownian motion, thermophoresis, and viscous dissipation are taken into account. The stretching velocity is assumed to vary linearly with the distance from the stagnation point. The fluid is electrically conducted with uniform magnetic field, and the work done due to deformation is taken into consideration. The three-coupled partial differential boundary layer equations are reduced to ordinary differential equations by using proper similarity transformations. Analytical solution by homotopy analysis method is obtained. Effects of different physical parameters on the dynamics of the problem are analyzed and discussed.

Keywords Non-Newtonian fluid · Third-grade fluid · Homotopy analysis method · Stretching sheet · Boundary layer equations

List of symbols

A_i	Kinematic tensors (–)
a, c	Positive constants (s^{-1})
\mathbf{B}	Magnetic field vector (T)
Bi	Biot number (–)
B_0	Magnetic field component (T)
b	Body forces ($N\ m^{-3}$)
C	Nanoparticles concentration ($kg\ m^{-3}$)
C_∞	Ambient fluid concentration ($kg\ m^{-3}$)
C_f	Skin friction coefficient (–)
D_B	Brownian diffusion coefficient ($m^2\ s^{-1}$)
D_T	Thermophoresis diffusion coefficient ($m^2\ s^{-1}$)
Ec	Eckert number (–)
f	Dimensionless velocity function (–)
g	Gravity acceleration ($m\ s^{-2}$)
G_T	Local Grashof number (–)
h_f	Convection coefficient ($W\ m^{-2}K^{-1}$)
\mathbf{j}	Electric current (A)
K	Viscoelastic parameter (–)
k^*	Mean absorption coefficient (–)
L	Cross-viscous parameter (–)

M	Magnetic field parameter (–)
Nb	Brownian motion parameter (–)
Nt	Thermophoresis parameter (–)
Nu_x	Local Nusselt number (–)
Pr	Prandtl number (–)
Re_x	Local Reynolds number (–)
R_d	Radiation parameter (–)
\mathbf{T}	Cauchy stress tensor (–)
T_f	Hot fluid temperature (K)
T_∞	Ambient temperature (K)
U_∞	External flow velocity ($m\ s^{-1}$)
(u, v)	Velocity components ($m\ s^{-1}$)
u_w	Stretching sheet velocity ($m\ s^{-1}$)
(x, y)	Cartesian coordinate components (m)

Greek symbols

α	Thermal diffusivity ($m^2\ s^{-1}$)
α_i, β_i	Material constants (–)
β	Third-grade fluid parameter (–)
β_c	Coefficient of mass expansion (K^{-1})
β_T	Coefficient of thermal expansion (K^{-1})
ϕ	Dimensionless concentration function (–)
η	Similarity variable (–)
μ	Viscosity ($N\ s\ m^{-2}$)
ν	Kinematic viscosity ($m^2\ s^{-1}$)
θ	Dimensionless temperature function (–)

✉ Asghar B. Rahimi
rahimiab@um.ac.ir

¹ Faculty of Mechanical Engineering, Ferdowsi University of Mashhad, P.O. Box No. 91775-1111, Mashhad, Iran

ρ	Density (kg m^{-3})
ρ_f	Density of the base fluid (kg m^{-3})
ρ_p	Density of the nanoparticles (kg m^{-3})
σ	Electrical conductivity of fluid (S m^{-1})
σ^*	Stefan–Boltzmann constant ($\text{W m}^{-2} \text{K}^{-4}$)

Introduction

The boundary layer flow near stretching sheet has many industrial and engineering applications, for example, extrusion of plastic, paper production, hot rolling, polymer processing, and metallurgical processes. Many authors have studied the problem of flow and heat transfer over stretching sheet. Sakiadis [1, 2] first worked on a two-dimensional flow on a continuous flat solid surface and axisymmetric flow on a continuous cylindrical solid surface. Erickson et al. [3] considered energy and diffusion equations and solved them numerically. Ali and Yousef [4] studied the boundary layer flow over a uniformly moving vertical surface with suction or injection. Similarity solution was obtained, and governing equations were solved numerically. Analysis of mixed convection in boundary layers on a vertically, continuous stretching sheet was presented by Chen [5]. He used numerical methods to solve the problem. Ali [6] studied the effect of temperature-dependent viscosity on laminar mixed convection flow on a continuously moving vertical surface, numerically. Further, Ishak et al. [7] presented steady mixed convection boundary layer flow near the two-dimensional stagnation-point flow of a viscous fluid over a stretching vertical sheet. Ishak et al. [8] worked on MHD stagnation-point flow toward a stretching sheet. Hayat et al. [9] presented two-dimensional mixed convection boundary layer MHD stagnation-point flow through a porous medium bounded by a stretching vertical plate and took radiation into account.

The idea of using solid particles in fluid in order to increase thermal conductivity of base fluid first introduced by Masuda et al. [10]. Chol [11] used the term “nanofluids” for fluids that suspended metallic nanoparticles in conventional heat transfer fluids to enhance base fluids heat transfer properties. He showed that one of the benefits of nanofluids is reductions in heat exchanger pumping power. Unlike traditional fluids which the thermophoresis effects are negligible in force convection flows, Buongiorno [12] suggested a mathematical model for nanofluids by considering Brownian diffusion and thermophoresis to have the most important slip mechanisms in nanofluids. Brownian motion is the random motion of nanoparticles suspended in a base fluid resulting from their collisions with the fast-moving molecules in the fluid. Thermophoresis is a phenomenon observed in mixtures of moving particles

where the different particle types exhibit different responses to the force of a temperature gradient because of their different thermophysical properties. In the governing equations for nanofluids, nanoparticle concentration depends on temperature mostly by thermophoresis and temperature depends on nanoparticle concentration by Brownian and thermophoresis terms. This kind of fluids has many applications, such as cooling electronics pieces, heat exchangers, and many others which have attracted the interest of the researchers. Khan and Pop [13] studied the flow of nanofluid over a stretching sheet, numerically. Haq et al. [14] investigated flow of nanofluid over a stretching sheet and they considered effects of radiation, thermal, and velocity slip on flow characteristics. In their study, they used a numerical method to solve three-coupled equations governing the problem. Makinde and Aziz [15] studied flow of a nanofluid past a stretching sheet with convective boundary condition and solved it numerically. For similarity solution of boundary layer flow with convective boundary, see Aziz [16]. HAM solution of stagnation-point flow over stretching sheet was done by Mustafa et al. [17]. There are many works done in the literature which considers flow of nanofluids over stretching sheet with variety of boundary conditions and parameters involved, see [18–25] and more recent article by Malvandi et al. [26]. They studied mixed convection of nanofluid in a micro-annuli and used Buongiorno’s model to study nanofluid and nanoparticle migrations into the base fluid and considered effects of magnetic field and temperature-dependent properties on the flow. As mentioned in the paper, ignoring the temperature dependency of the thermophysical properties does not affect the flow and heat transfer characteristics of the nanofluids significantly. Therefore, in the present study, thermophysical properties such as thermal conductivity and viscosity are assumed to be constant. Moreover, there are other works in the literature which are considering nanofluids and its applications in different geometries. Rashidi et al. [27] performed a review of applications of nanofluids in condensing and evaporating systems. They studied advantages and disadvantages of using nanofluids in these systems. In this review, they show that the nanoparticle deposition and nanoparticle suspension are two important factors affecting the thermal system’s efficiency. Javadi et al. [28] studied Al_2O_3 water nanofluid flow and convective heat transfer around a square obstacle with consideration of various incidence angles. They found that incidence angle has influence on heat transfer rate of the flow. In an interesting research, Bovand et al. [29] worked on optimum interactions between using nanofluids and magnetic field in a flow around a triangular obstacle in order to control heat transfer rate of the flow. They used response surface methodology (RSM) to optimize and control the interactions between

two techniques. They concluded that magnetic field parameter has more impact on heat transfer rate rather than nanoparticle's concentration. Shirejini et al. [30] considered flow and heat transfer around a rotating cylinder and investigate the effects of involving parameters such as nanoparticle concentration and Reynolds number on heat transfer rate of the flow. Akar et al. [31] performed a second law of thermodynamic analysis on the same problem and studied the influence of related parameters on the viscous and thermal entropy generations and Bejan number.

There are many substances which cannot be described by the classic linearly viscous fluid model such as liquid foams, polymeric fluids, food products, and slurries that have many industrial and engineering applications. In order to describe unconventional behavior of these fluids, many models have been suggested. The fluid of differential types [32] is one of the many models which has been used to describe non-Newtonian fluids. Fosdick and Rajagopal [33] studied thermodynamics and stability of fluids of third grade. Rajagopal et al. [34] discussed the force convection flow of an incompressible third-grade fluid past a porous plate subject to suction. Further, Maneschy et al. [35] extended the work of Rajagopal and considered heat transfer phenomena as well. They solved, simultaneously, the highly nonlinear momentum and the energy equations by Runge–Kutta method along with Newton–Raphson techniques. Further, one can cite works done by B. Sahoo and coauthors. In their works, they investigated boundary layer flow of a third-grade non-Newtonian fluid over an infinite plate [36] and exponentially stretching sheet [37] with considering partial slip effect and various thermal boundary conditions. Recently, Shehzad et al. [38] worked on two-dimensional boundary layer flow of an incompressible third-grade nanofluid over a stretching surface; in this work, they used Buongiorno's mathematical model to study nanofluid characteristics and solved the governing equations by using HAM. Hayat et al. [39, 40] examined MHD flow of second-grade nanofluid over a nonlinear stretching sheet with convective boundary condition and prescribed surface temperature. They solved these problems using HAM. Ghasemi et al. [41] used third-grade non-Newtonian nanofluid to study flow analysis of blood in porous arteries and magnetic field effects are considered. They applied two analytical methods, namely collocation method (CM) and optimal homotopy asymptotic method (OHAM) to solve the equations, and comparison between these two methods is given.

Many different methods have been introduced to solve nonlinear equations analytically such as homotopy analysis method that was introduced by Liao [42–44] which does not depend on a small parameter like perturbation techniques. In problems that concern non-Newtonian fluids, it's

possible that the order of the derivative in momentum equation gets higher [35] due to necessary manipulations. In numerical solution for such problems an extra boundary condition is needed in order to solve the equations, which is zero shear-stress at infinity for unbounded domains. As stated by Liao and Tan [45] in HAM solution, the order of linear operator is not related to the highest order of derivatives in equations, therefore, by choosing proper linear operator, boundary layer equations of non-Newtonian fluids can be solved without need of an extra boundary condition. Another advantage of using HAM instead of numerical methods is that in analytical solutions there is no need to choose a big enough number to represent infinity or boundary layer thickness that varies with different parameters existing in equations.

The study of boundary layer flow and heat transfer of non-Newtonian fluids over a stretching sheet has various applications in industrial processes for example in manufacturing and extraction of polymers and rubber sheets, paper production, drawing of plastic films and wires. Moreover, the concurrent utilization of heat and mass transfer in boundary layer flow of non-Newtonian fluids have more importance in electrochemical processes, insulation of nuclear reactors, petroleum reservoirs reactors, and many others. Since the processes mentioned above have very high working temperature, the radiation term plays an important role in the cooling or heating operation. In addition, using nanofluids and magnetic fields are two common methods used by researchers in order to control the heat transfer rate in such processes. The objective of the present article is to study mixed convection stagnation-point flow of a third-grade nanofluid over a vertical stretching sheet with convective boundary condition. Newly proposed condition for concentration has been used that is zero mass flux of nanoparticles at the surface. As it is stated by Kuznetsov and Nield [46], this new boundary condition is physically more realistic. Homotopy analysis method (HAM) is used to solve the three-coupled ordinary differential equations resulting in the problem. Graphical diagrams of different parameters of interest against velocity, temperature, and concentration distributions are presented and discussed. According to the review in the literature and as far as the authors' best knowledge, no one has yet considered this problem.

Mathematical formulation

Consider a steady, two-dimensional, incompressible, stagnation-point flow of a MHD third-grade nanofluid over a vertical stretching sheet. Two equal and opposite forces are applied to this sheet along the x -axis in such a way that the surface stretches with velocity $u_w = ax$ while the origin is

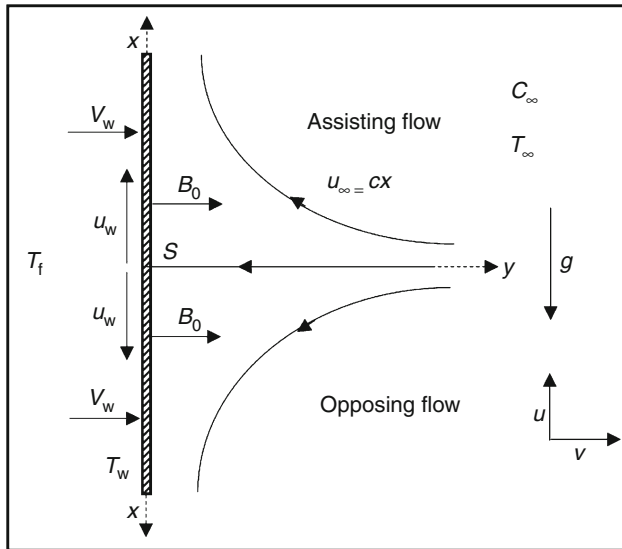


Fig. 1 Geometry of the problem

fixed at S , see Fig. 1. The fluid is electrically conducted due to constant magnetic field \mathbf{B}_0 which is applied in y -direction. Hall current and electric field effects are neglected due to the small magnetic Reynolds number. It is assumed that the fluid is at temperature T_∞ and the plate is heated by convection from a hot fluid at temperature T_f which is due to the heat transfer coefficient h_f . The flux of the nanoparticle fraction at the surface of the plate is assumed to be zero.

For an incompressible conducting fluid, the equations of motion and continuity considering body forces are:

$$\text{div } \mathbf{v} = 0 \tag{1}$$

$$\rho \frac{d\mathbf{v}}{dt} = \text{div} \mathbf{T} + \rho \mathbf{b} + \mathbf{J} \times \mathbf{B} \tag{2}$$

here ρ is density of the fluid which is assumed to be a constant, \mathbf{v} denotes the velocity field, \mathbf{b} stands for body forces, \mathbf{J} is the electric current, and \mathbf{T} is Cauchy stress that for an incompressible third-grade fluid is defined as [47]:

$$\mathbf{T} = -p\mathbf{I} + \mu\mathbf{A}_1 + \alpha_1\mathbf{A}_2 + \alpha_2\mathbf{A}_1^2 + \beta_1\mathbf{A}_3 + \beta_2(\mathbf{A}_1\mathbf{A}_2 + \mathbf{A}_2\mathbf{A}_1) + \beta_3(\text{tr}\mathbf{A}_1^2)\mathbf{A}_1 \tag{3}$$

where μ is viscosity coefficient, α_i and β_i are material moduli, and $\mathbf{A}_1, \mathbf{A}_2,$ and \mathbf{A}_3 are kinematic tensors as:

$$\mathbf{A}_1 = \mathbf{L} + (\mathbf{L})^T \tag{4}$$

$$\mathbf{A}_n = \frac{d}{dt}\mathbf{A}_{n-1} + \mathbf{A}_{n-1}\mathbf{L} + (\mathbf{L})^T\mathbf{A}_{n-1}, \quad n = 2, 3 \tag{5}$$

and

$$\mathbf{L} = \nabla \mathbf{v} \tag{6}$$

Here, $\frac{d}{dt}$ is material time derivative which is defined as:

$$\frac{d()}{dt} = \frac{\partial()}{\partial t} + \mathbf{v} \cdot \nabla() \tag{7}$$

As stated by Fosdick and Rajagopal, for a thermodynamically compatible fluid that meets Clausius–Duhem inequality the following relation is used:

$$\mu \geq 0, \quad \alpha_1 \geq 0, \quad \beta_1 = \beta_2 = 0, \quad \beta_3 \geq 0, \quad |\alpha_1 + \alpha_2| \leq \sqrt{24\mu\beta_3} \tag{8}$$

$$\mathbf{T} = -p\mathbf{I} + \mu\mathbf{A}_1 + \alpha_1\mathbf{A}_2 + \alpha_2\mathbf{A}_1^2 + \beta_3(\text{tr}\mathbf{A}_1^2)\mathbf{A}_1 \tag{9}$$

By considering the work done due to deformation, radiation and using Boussinesq and usual boundary layer approximations from Pakdemirli [48] the governing equations of continuity, momentum, energy, and concentration, respectively, are:

$$\frac{\partial u}{\partial x} + \frac{\partial v}{\partial y} = 0 \tag{10}$$

$$\begin{aligned} u \frac{\partial u}{\partial x} + v \frac{\partial u}{\partial y} &= v \frac{\partial^2 u}{\partial y^2} + U_\infty \frac{dU_\infty}{dx} \\ &+ \frac{\alpha_1}{\rho} \left(u \frac{\partial^3 u}{\partial x \partial y^2} + \frac{\partial u}{\partial x} \frac{\partial^2 u}{\partial y^2} + 3 \frac{\partial u}{\partial y} \frac{\partial^2 v}{\partial y^2} + v \frac{\partial^3 u}{\partial y^3} \right) \\ &+ \frac{2\alpha_2}{\rho} \frac{\partial u}{\partial y} \frac{\partial^2 v}{\partial y^2} + \frac{6\beta_3}{\rho} \left(\frac{\partial u}{\partial y} \right)^2 \frac{\partial^2 u}{\partial y^2} \\ &- \frac{\sigma B_0^2}{\rho} (u - U_\infty) \pm g\beta_T (T - T_\infty) \pm g\beta_C (C - C_\infty) \end{aligned} \tag{11}$$

$$\begin{aligned} u \frac{\partial T}{\partial x} + v \frac{\partial T}{\partial y} &= \alpha \frac{\partial^2 T}{\partial y^2} + \frac{(\rho c_p)_p}{(\rho c_p)_f} \left(D_B \frac{\partial T}{\partial y} \frac{\partial C}{\partial y} + \frac{D_T}{T_\infty} \left(\frac{\partial T}{\partial y} \right)^2 \right) \\ &+ \frac{\mu}{(\rho c_p)_f} \left(\frac{\partial u}{\partial y} \right)^2 - \frac{1}{(\rho c_p)_f} \frac{\partial q_r}{\partial y} \\ &+ \frac{\sigma B_0^2}{(\rho c_p)_f} (u - U_\infty)^2 + \frac{\alpha_1}{(\rho c_p)_f} \left(u \frac{\partial u}{\partial y} \frac{\partial^2 u}{\partial x \partial y} \right. \\ &\left. + v \frac{\partial u}{\partial y} \frac{\partial^2 u}{\partial y^2} \right) + \frac{2\beta_3}{(\rho c_p)_f} \left(\frac{\partial u}{\partial y} \right)^4 \end{aligned} \tag{12}$$

$$u \frac{\partial C}{\partial x} + v \frac{\partial C}{\partial y} = D_B \frac{\partial^2 C}{\partial y^2} + \frac{D_T}{T_\infty} \frac{\partial^2 T}{\partial y^2} \tag{13}$$

In above equations, u and v are velocity components along the x - and y -axes, respectively, U_∞ is external flow velocity, T is fluid temperature, T_∞ is ambient temperature, C is nanoparticle concentration, $(\rho c_p)_p$ is particle heat capacity and $(\rho c_p)_f$ is fluid heat capacity, g is gravity acceleration, $\alpha, \nu, \beta_T,$ and β_C are thermal diffusivity, kinematic viscosity, and coefficient of thermal and mass expansion, respectively, D_B is the Brownian diffusion coefficient, and D_T is the thermophoresis diffusion coefficient. The signs “+” and “−” correspond to assisting and

opposing buoyant flow, respectively, and σ is the electrical conductivity of the fluid.

By using Rosseland approximation, the radiation heat flux is given by:

$$q_r = -\frac{4\sigma^*}{3k^*} \frac{\partial T^4}{\partial y} \tag{14}$$

where σ^* and k^* are Stefan–Boltzmann and the mean absorption coefficients, respectively. By expanding T^4 about T_∞ in Taylor’s series and neglecting the higher order terms, we have:

$$T^4 \cong 4T_\infty^3 T - 3T_\infty^4 \tag{15}$$

Substituting (14), (15) in (12) the energy equation becomes:

$$\begin{aligned} u \frac{\partial T}{\partial x} + v \frac{\partial T}{\partial y} = & \alpha \frac{\partial^2 T}{\partial y^2} + \frac{(\rho c_p)_p}{(\rho c_p)_f} \left(D_B \frac{\partial T}{\partial y} \frac{\partial C}{\partial y} + \frac{D_T}{T_\infty} \left(\frac{\partial T}{\partial y} \right)^2 \right) \\ & + \frac{\mu}{(\rho c_p)_f} \left(\frac{\partial u}{\partial y} \right)^2 + \frac{16\sigma^* T_\infty^3}{3\rho c_p k^*} \frac{\partial^2 T}{\partial y^2} \\ & + \frac{\sigma B_0^2}{(\rho c_p)_f} (u - U_\infty)^2 \\ & + \frac{\alpha_1}{(\rho c_p)_f} \left(u \frac{\partial u}{\partial y} \frac{\partial^2 u}{\partial x \partial y} + v \frac{\partial u}{\partial y} \frac{\partial^2 u}{\partial y^2} \right) \\ & + \frac{2\beta_3}{(\rho c_p)_f} \left(\frac{\partial u}{\partial y} \right)^4 \end{aligned} \tag{16}$$

The subjected boundary conditions are:

$$u = u_w(x) = ax, \quad v = 0, \quad -k \frac{\partial T}{\partial y} = h_f(T_f - T), \tag{17}$$

$$D_B \frac{\partial C}{\partial y} + \frac{D_T}{T_\infty} \frac{\partial T}{\partial y} = 0 \quad \text{at } y = 0$$

$$u = u_\infty(x) = cx, \quad \frac{\partial u}{\partial y} = 0, \quad T \rightarrow T_\infty, \quad C \rightarrow C_\infty \tag{18}$$

as $y \rightarrow \infty$

Suitable similarity transformations are defined as, Ref [17]:

$$\begin{aligned} \psi &= \sqrt{av}xf(\eta), \quad \eta = \sqrt{\frac{a}{v}}y, \quad u = \frac{\partial \psi}{\partial y} = axf'(\eta) \\ v &= -\frac{\partial \psi}{\partial x} = -\sqrt{av}f(\eta), \quad \theta(\eta) = \frac{T - T_\infty}{T_f - T_\infty}, \tag{19} \\ \phi(\eta) &= \frac{C - C_\infty}{C_\infty} \end{aligned}$$

using above relations, the continuity Eq. (10) is satisfied automatically and Eqs. (11), (13) and (16)–(18) become the following system of ordinary differential equations:

$$\begin{aligned} f''' + ff'' - f'^2 + \frac{c^2}{a^2} + K(2f'f''' - ff^{(iv)}) - (3K + 2L)f''^2 \\ + 6\beta Re_x f''' f''^2 + M\left(\frac{c}{a} - f'\right) \pm Br\phi \pm Gr\theta = 0 \end{aligned} \tag{20}$$

$$\begin{aligned} \left(\frac{1}{Pr} + \frac{4}{3}R_d\right)\theta'' + f\theta' + Nb\theta'\phi' + Nt\theta'^2 + Ec f''^2 \\ + M \cdot Ec \left(f' - \frac{c}{a}\right)^2 + K \cdot Ec (f'f''^2 - ff''f''') \\ + 2Ec \cdot \beta \cdot Re_x f''^4 = 0 \end{aligned} \tag{21}$$

$$\phi'' + Le \cdot Pr \cdot f\phi' + \frac{Nt}{Nb}\theta'' = 0 \tag{22}$$

with boundary conditions:

$$\begin{aligned} f = 0, \quad f' = 0, \quad \theta' = -Bi(1 - \theta), \quad Nb\phi' + Nt\theta' = 0 \\ \text{at } \eta = 0 \end{aligned} \tag{23}$$

$$f' = \frac{c}{a}, \quad \theta = 0, \quad \phi = 0 \quad \text{as } \eta \rightarrow \infty \tag{24}$$

Here, prime denotes differentiation with respect to η , and the other dimensionless parameters are defined as follows:

$$\begin{aligned} M &= \frac{\sigma B_0^2}{\rho a}, \quad G_T = \frac{gx^3 \beta_T (T_f - T_\infty)}{v^2 Re_x^2}, \quad B_T = \frac{gx^3 \beta_c C_\infty}{v^2 Re_x^2}, \\ Pr &= \frac{v}{\alpha}, \quad Le = \frac{\alpha}{D_B} \\ Ec &= \frac{u_\infty^2}{c_p(T_f - T_\infty)}, \quad R_d = \frac{4T_\infty^3 \sigma^*}{k^* k_f}, \quad Nb = \frac{(\rho c_p)_p D_B C_\infty}{(\rho c_p)_f v}, \\ Bi &= \frac{h_f}{k} \sqrt{\frac{v}{a}} \\ Nt &= \frac{(\rho c_p)_p D_B (T_f - T_\infty)}{(\rho c_p)_f v T_\infty}, \quad K = \frac{a\alpha_1}{\mu}, \quad L = \frac{a\alpha_2}{\mu}, \quad \beta = \frac{a^2 \beta_3}{\mu} \end{aligned} \tag{25}$$

M is magnetic field parameter, G_T is local Grashof number, Bi represents Biot number, Ec stands for Eckert number, R_d is radiation parameter, Nb and Nt are the Brownian motion and thermophoresis parameter, respectively, K is viscoelastic parameter, L stands for cross-viscous parameter, β stands for the third-grade fluid parameter, and Le represents Lewis number.

The skin friction coefficient C_f and the local Nusselt number Nu_x definitions are

$$C_f = \frac{\tau_w}{\rho u_w^2}, \quad Nu_x = \frac{xq_w}{k(T_f - T_\infty)} \tag{26}$$

where for third-grade fluid

$$\tau_w = \left[\frac{\partial u}{\partial y} + \frac{\alpha_1}{\mu} \left(2 \frac{\partial u}{\partial x} \frac{\partial u}{\partial y} + v \frac{\partial^2 u}{\partial y^2} + u \frac{\partial^2 u}{\partial x \partial y} \right) + \frac{2\beta_3}{\mu} \left(\frac{\partial u}{\partial y} \right)^3 \right]_{y=0} \tag{27}$$

and

$$q_w = \left[-k \frac{\partial T}{\partial y} - \frac{16\sigma^* T_\infty^3}{3k^*} \frac{\partial T}{\partial y} \right]_{y=0} \tag{28}$$

By using similarity transformations (19), the expression for dimensionless skin friction and local Nusselt number becomes

$$C_f Re_x^{1/2} = 2 \left[f''(0) + K(3f'(0)f''(0) - f(0)f'''(0)) + 2\beta Re_x f''(0)^3 \right] \tag{29}$$

$$Nu_x Re_x^{-1/2} = - \left(1 + \frac{4}{3} R_d \right) \theta'(0) a \tag{30}$$

Due to the boundary condition for concentration, the dimensionless mass flux represented by a Sherwood number Sh_x is now identically zero.

Series solution by homotopy analysis method (HAM)

Now we want to solve the three-coupled ordinary differential Eqs. (20)–(22) subjected to the boundary conditions (23) and (24) by using HAM. First, we must choose initial guesses and auxiliary linear operators for homotopic solution which are, respectively:

$$f_0(\eta) = \frac{c}{a} \eta + \left(1 - \frac{c}{a} \right) (1 - e^{-\eta}), \quad \theta_0(\eta) = \frac{Bi}{Bi + 1} e^{-\eta}, \quad \phi_0(\eta) = - \frac{Nt}{Nb Bi + 1} e^{-\eta} \tag{31}$$

$$\mathbf{L}_f = f''' - f', \quad \mathbf{L}_\theta = \theta'' - \theta, \quad \mathbf{L}_\phi = \phi'' - \phi \tag{32}$$

and must satisfy the boundary conditions. The auxiliary linear operators above have the following properties:

$$\mathbf{L}_f [C_1 + C_2 e^\eta + C_3 e^{-\eta}] = 0, \quad \mathbf{L}_\theta [C_4 e^\eta + C_5 e^{-\eta}] = 0, \quad \mathbf{L}_\phi [C_6 e^\eta + C_7 e^{-\eta}] = 0 \tag{33}$$

where $C_1 - C_7$ are arbitrary constants. Let h_f, h_θ, h_ϕ denote nonzero auxiliary parameters and $H_f(\eta), H_\theta(\eta), H_\phi(\eta)$ denote auxiliary functions, then the zeroth-order deformation equations are:

$$\begin{aligned} (1-p)\mathbf{L}_f [\hat{f}(\eta, p) - f_0(\eta)] &= p h_f H_f(\eta) \mathbf{N}_f [\hat{f}(\eta, p), \hat{\theta}(\eta, p), \hat{\phi}(\eta, p)] \\ (1-p)\mathbf{L}_\theta [\hat{\theta}(\eta, p) - \theta_0(\eta)] &= p h_\theta H_\theta(\eta) \mathbf{N}_\theta [\hat{f}(\eta, p), \hat{\theta}(\eta, p), \hat{\phi}(\eta, p)] \\ (1-p)\mathbf{L}_\phi [\hat{\phi}(\eta, p) - \phi_0(\eta)] &= p h_\phi H_\phi(\eta) \mathbf{N}_\phi [\hat{f}(\eta, p), \hat{\theta}(\eta, p), \hat{\phi}(\eta, p)] \end{aligned} \tag{34}$$

where $p \in [0, 1]$ denotes the embedding parameter and it is obvious that when $p = 0$:

$$\hat{f}(\eta, 0) = f_0, \quad \hat{\theta}(\eta, 0) = \theta_0, \quad \hat{\phi}(\eta, 0) = \phi_0 \tag{35}$$

When p increases from 0 to 1, $\hat{f}(\eta, 0), \hat{\theta}(\eta, 0), \hat{\phi}(\eta, 0)$ varies from initial approximations to the original equations so that we have

$$\hat{f}(\eta, 1) = f(\eta), \quad \hat{\theta}(\eta, 1) = \theta(\eta), \quad \hat{\phi}(\eta, 1) = \phi(\eta) \tag{36}$$

From (20)–(22) and (23), (24) we define the nonlinear operators:

$$\begin{aligned} \mathbf{N}_f [\hat{f}(\eta, p), \hat{\theta}(\eta, p), \hat{\phi}(\eta, p)] &= \frac{\partial^3 \hat{f}}{\partial \eta^3} + \hat{f} \frac{\partial^2 \hat{f}}{\partial \eta^2} - \left(\frac{\partial \hat{f}}{\partial \eta} \right)^2 + \frac{c^2}{a^2} \\ &+ K \left(2 \frac{\partial \hat{f}}{\partial \eta} \frac{\partial^3 \hat{f}}{\partial \eta^3} - \hat{f} \frac{\partial^4 \hat{f}}{\partial \eta^4} \right) - (3K + 2L) \left(\frac{\partial^2 \hat{f}}{\partial \eta^2} \right)^2 \\ &+ 6\beta Re_x \frac{\partial^3 \hat{f}}{\partial \eta^3} \left(\frac{\partial^2 \hat{f}}{\partial \eta^2} \right)^2 + M \left(\frac{c}{a} - \frac{\partial \hat{f}}{\partial \eta} \right) \pm Br \hat{\phi} \pm Gr \hat{\theta} \end{aligned} \tag{37}$$

$$\begin{aligned} \mathbf{N}_\theta [\hat{f}(\eta, p), \hat{\theta}(\eta, p), \hat{\phi}(\eta, p)] &= \left(\frac{1}{Pr} + \frac{4}{3} R_d \right) \frac{\partial^2 \hat{\theta}}{\partial \eta^2} + \hat{f} \frac{\partial \hat{\theta}}{\partial \eta} + Nb \frac{\partial \hat{\theta}}{\partial \eta} \frac{\partial \hat{\phi}}{\partial \eta} \\ &+ Nt \left(\frac{\partial \hat{\theta}}{\partial \eta} \right)^2 + Ec \left(\frac{\partial^2 \hat{f}}{\partial \eta^2} \right)^2 + M \cdot Ec \left(\frac{c}{a} - \frac{\partial \hat{f}}{\partial \eta} \right)^2 \\ &+ K \cdot Ec \left(\frac{\partial \hat{f}}{\partial \eta} \left(\frac{\partial^2 \hat{f}}{\partial \eta^2} \right)^2 - \hat{f} \frac{\partial \hat{f}}{\partial \eta} \frac{\partial^2 \hat{f}}{\partial \eta^2} \right) \\ &+ 2Ec \cdot \beta \cdot Re_x \left(\frac{\partial^2 \hat{f}}{\partial \eta^2} \right)^4 \end{aligned} \tag{38}$$

$$\begin{aligned} \mathbf{N}_\phi [\hat{f}(\eta, p), \hat{\theta}(\eta, p), \hat{\phi}(\eta, p)] &= \frac{\partial^2 \hat{\phi}}{\partial \eta^2} + Le \cdot Pr \cdot \hat{f} \frac{\partial \hat{\phi}}{\partial \eta} + \frac{Nt}{Nb} \frac{\partial^2 \hat{\theta}}{\partial \eta^2} \end{aligned} \tag{39}$$

subjected to the boundary conditions:

$$\begin{aligned} \hat{f}(0,p) = 0, \quad \hat{f}'(0,p) = 1, \quad \hat{f}'(\infty,p) = \frac{c}{a}, \\ \hat{\theta}'(0,p) = -Bi(1 - \hat{\theta}(0,p)) \\ \hat{\theta}(\infty,p) = 0, \quad Nb\hat{\phi}'(0,p) + Nt\hat{\theta}'(0,p) = 0, \quad \hat{\phi}(\infty,p) = 0 \end{aligned} \tag{40}$$

Expanding $\hat{f}(\eta,p)$, $\hat{\theta}(\eta,p)$, $\hat{\phi}(\eta,p)$ in Taylor's series about the embedding parameter p , we have:

$$\hat{f}(\eta,p) = f_0(\eta) + \sum_{m=1}^{\infty} f_m(\eta)p^m, \quad f_m(\eta) = \left. \frac{1}{m!} \frac{\partial^m \hat{f}(\eta,p)}{\partial p^m} \right|_{p=0} \tag{41}$$

$$\begin{aligned} \hat{\theta}(\eta,p) = \theta_0(\eta) + \sum_{m=1}^{\infty} \theta_m(\eta)p^m, \\ \theta_m(\eta) = \left. \frac{1}{m!} \frac{\partial^m \hat{\theta}(\eta,p)}{\partial p^m} \right|_{p=0} \end{aligned} \tag{42}$$

$$\begin{aligned} \hat{\phi}(\eta,p) = \phi_0(\eta) + \sum_{m=1}^{\infty} \phi_m(\eta)p^m, \\ \phi_m(\eta) = \left. \frac{1}{m!} \frac{\partial^m \hat{\phi}(\eta,p)}{\partial p^m} \right|_{p=0} \end{aligned} \tag{43}$$

Assume that the auxiliary parameters h_f, h_θ, h_ϕ and auxiliary functions $H_f(\eta), H_\theta(\eta), H_\phi(\eta)$ are properly chosen so that the series converge at $p = 1$, then the solutions become:

$$f(\eta) = f_0(\eta) + \sum_{m=1}^{\infty} f_m(\eta) \tag{44}$$

$$\theta(\eta) = \theta_0(\eta) + \sum_{m=1}^{\infty} \theta_m(\eta) \tag{45}$$

$$\phi(\eta) = \phi_0(\eta) + \sum_{m=1}^{\infty} \phi_m(\eta) \tag{46}$$

Differentiating the zero-order deformation Eq. (34) m times about p , and setting $p = 0$, and finally dividing them by $m!$, we obtain the m th-order deformation equations as:

$$\mathbf{L}_f[f_m(\eta) - \chi_m f_{m-1}(\eta)] = h_f H_f(\eta) \mathbf{R}_f^m(\eta) \tag{47}$$

$$\mathbf{L}_\theta[\theta_m(\eta) - \chi_m \theta_{m-1}(\eta)] = h_\theta H_\theta(\eta) \mathbf{R}_\theta^m(\eta) \tag{48}$$

$$\mathbf{L}_\phi[\phi_m(\eta) - \chi_m \phi_{m-1}(\eta)] = h_\phi H_\phi(\eta) \mathbf{R}_\phi^m(\eta) \tag{49}$$

subjected to the boundary conditions

$$\begin{aligned} f_m(0) = f'_m(0) = f'_m(\infty) = 0, \quad \theta_m(\infty) = \phi_m(\infty) = 0 \\ Nb\phi'_m(0) + Nt\theta'_m(0) = 0, \quad \theta'_m(0) - Bi\theta_m(0) = 0 \end{aligned} \tag{50}$$

where

$$\chi_m = \begin{cases} 0 & m \leq 1 \\ 1 & m > 1 \end{cases} \tag{51}$$

and

$$\begin{aligned} \mathbf{R}_f^m(\eta) = f'''_{m-1} - Mf'_{m-1} \pm Br\phi_{m-1} \pm Gr\theta_{m-1} \\ + (1 - \chi_m) \left(M\frac{c}{a} + \frac{c^2}{a^2} \right) \\ + K \sum_{k=0}^{m-1} \left(2f'_{m-1-k} f'''_k - f_{m-1-k} f^{(iv)}_k \right) \\ - (3K + 2L) \sum_{k=0}^{m-1} f''_{m-1-k} f''_k \end{aligned} \tag{52}$$

$$\begin{aligned} \mathbf{R}_\theta^m(\eta) = \left(\frac{1}{Pr} + \frac{4}{3}R_d \right) \theta''_{m-1} - 2M \cdot Ec \frac{c}{a} f'_{m-1} \\ + (1 - \chi_m) M \cdot Ec \frac{c^2}{a^2} + \sum_{k=0}^{m-1} f_{m-1-k} \theta'_k \\ + Nb \sum_{k=0}^{m-1} \theta'_{m-1-k} \phi'_k + Nt \sum_{k=0}^{m-1} \theta'_{m-1-k} \theta'_k + Ec \sum_{k=0}^{m-1} f''_{m-1-k} f''_k \\ K \cdot Ec \left(\sum_{k=0}^{m-1} f'_{m-1-k} \sum_{i=0}^k f''_{k-i} f''_i - \sum_{k=0}^{m-1} f_{m-1-k} \sum_{i=0}^k f''_{k-i} f'''_i \right) \\ + 2Ec \cdot \beta \cdot Re_x \left(\sum_{k=0}^{m-1} f''_{m-1-k} \sum_{i=0}^k f''_{k-i} \sum_{j=0}^i f''_{i-j} f''_j \right) \end{aligned} \tag{53}$$

$$\mathbf{R}_\phi^m(\eta) = \phi''_{m-1} + \frac{Nt}{Nb} \theta''_{m-1} + Le \cdot Pr \sum_{k=0}^{m-1} f_{m-1-k} \phi'_k \tag{54}$$

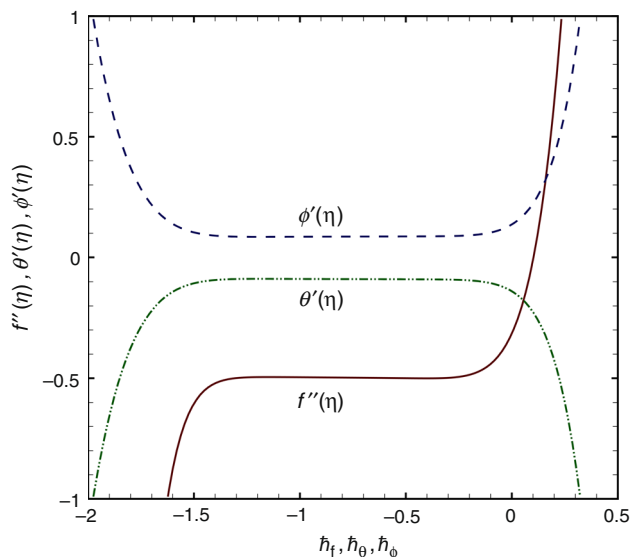


Fig. 2 h -curves for $f(\eta)$, $\theta(\eta)$, $\phi(\eta)$ when $c/a = 0.5$

Table 1 Convergence of the solution in different order of approximations when $c/a = 1$

Order of approximations	$-f''(0)$	$-\theta'(0)$	$\phi'(0)$
1	-6.712×10^{-18}	0.0870	0.0870
5	0.00936	0.0857	0.0857
10	0.00937	0.0858	0.0858
15	0.00937	0.0860	0.0860
25	0.00937	0.0860	0.0860

We set the auxiliary functions as

$$H_f(\eta) = e^{-\eta}, \quad H_\theta(\eta) = e^{-\eta}, \quad H_\phi(\eta) = e^{-\eta} \tag{55}$$

Then the common solutions are

$$f_m(\eta) = f_m^*(\eta) + C_1 + C_2e^\eta + C_3e^{-\eta} \tag{56}$$

$$\theta_m(\eta) = \theta_m^*(\eta) + C_4e^\eta + C_5e^{-\eta} \tag{57}$$

$$\phi_m(\eta) = \phi_m^*(\eta) + C_6e^\eta + C_7e^{-\eta} \tag{58}$$

where the integral constants are determined by using the boundary conditions (50):

$$C_2 = C_4 = C_6 = 0, \quad C_1 = -f_m^*(0) - \left. \frac{df_m^*}{d\eta} \right|_{\eta=0}, \quad C_3 = -\left. \frac{df_m^*}{d\eta} \right|_{\eta=0},$$

$$C_5 = \frac{\left. \frac{d\theta_m^*}{d\eta} \right|_{\eta=0} - Bi\theta_m^*(0)}{Bi + 1}, \quad C_7 = \frac{d\phi_m^*}{d\eta} \Big|_{\eta=0} - \frac{Nr}{Nb} \left(C_5 - \left. \frac{d\theta_m^*}{d\eta} \right|_{\eta=0} \right) \tag{59}$$

Convergence of HAM solution

As noted by Liao, solutions that are given by HAM (44)–(46) consist of nonzero auxiliary parameters h_f, h_θ, h_ϕ that convergence of the solution depends on them. If these

parameters are properly chosen, the given solution would be valid. In order to find appropriate ranges for these auxiliary parameters, the h -curves are drawn for 15th order of approximations. From Fig. 2, it is clear that the acceptable ranges are $[-1.3, -0.3]$ for h_f , $[-1.4, -0.2]$ for h_θ and h_ϕ . From Table 1, we can see that the HAM solution is convergent at 15th order of approximations and the values are accurate enough for this problem.

Discussions and results

In this section, graphical results of analytical solution will be shown in order to compare effects of different values of dimensionless parameters on flow characteristics. The default values of parameters in all figures are fixed as $c/a = 1$ and $Nb = Nr = 0.2, Pr = Le = K = L = \beta = Re_x = 1, M = Gr = Br = Rd = 0.5, Ec = Bi = 0.1$ unless otherwise stated. In order to have a better visualization of differences, we depict diagrams in some cases with $c/a = 0.5$ or $c/a = 2$ because in default case ($c/a = 1$), some of non-dimensional parameters have very small impact on distributions and thus the differences can't be seen visually.

In Figs. 3–26, effects of different dimensionless parameters on velocity $f'(\eta)$, temperature $\theta(\eta)$, and nanoparticle concentrations $\phi(\eta)$ are shown. Velocity distributions for different values of velocity ratio are shown in Fig. 3. It is obvious from this figure that for $c/a < 1$ the stretching velocity of the plate is more than the ambient velocity and when $c/a > 1$ the opposite behavior can be expected. When $c/a = 1$, the ambient fluid particles and plate move at the same velocity and only buoyant forces have slight impact on the velocity distribution. In this case,

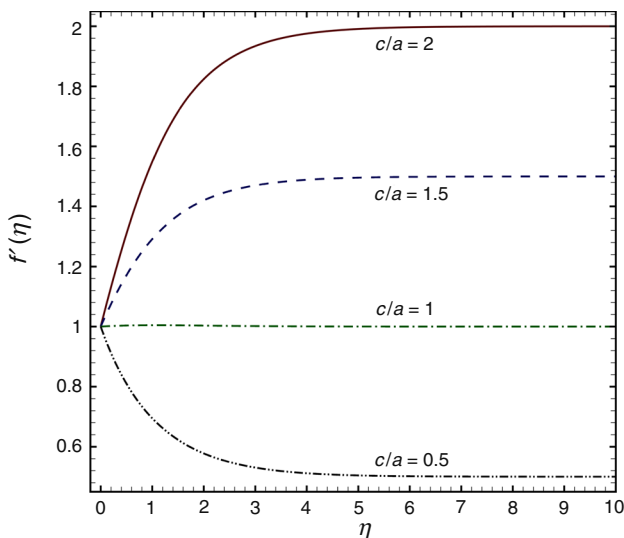


Fig. 3 Velocity profiles for different values of c/a

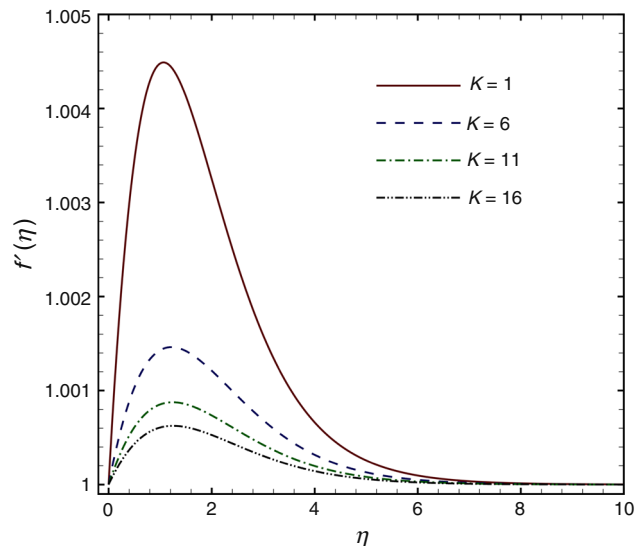


Fig. 4 Effects of K on velocity distribution

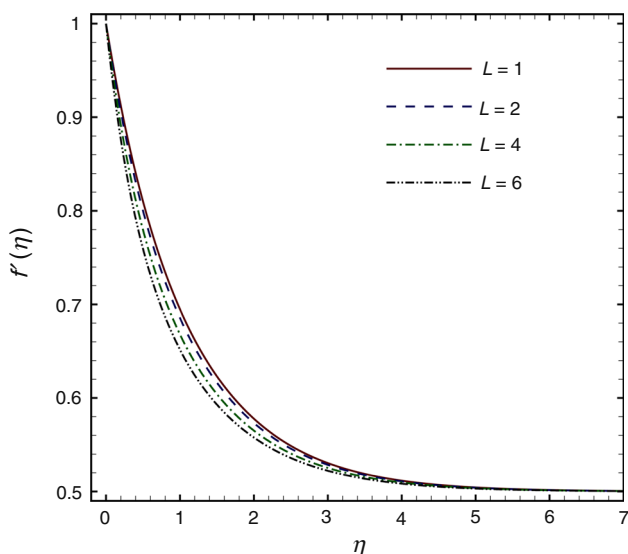


Fig. 5 Effects of L on velocity distribution with $c/a = 0.5$

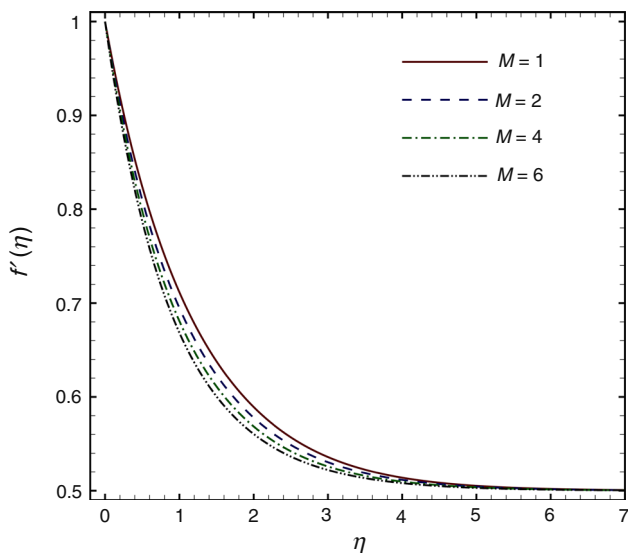


Fig. 6 Effects of M on velocity distribution with $c/a = 0.5$

the flow is just like natural convection. In Fig. 4, velocity distributions have been presented with different values of viscoelastic parameters. It is seen that velocity profiles $f'(\eta)$ decrease with increasing K and as a result boundary layer thickness increases. Figure 5 depicts the influence of cross-viscous parameter on the velocity profiles which are decreasing with increasing L and thus the momentum boundary layer thickness decreases. Same effect can be seen with magnetic field parameter M which is shown in Fig. 6. When a magnetic field is applied to an electrically conducting fluid, it causes a body force that acts transverse to magnetic field direction and as a result the velocity of the fluid decreases. In Figs. 7 and 8, variation of Gr and Br on velocity profiles is depicted when $c/a = 1$. It is clear

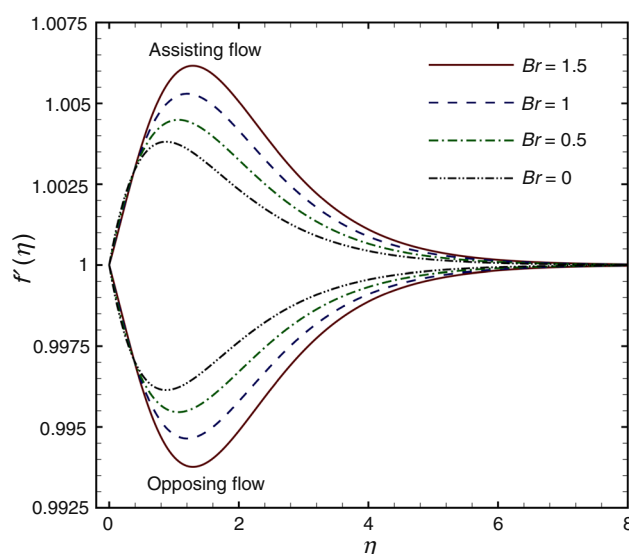


Fig. 7 Effects of Br on velocity distribution

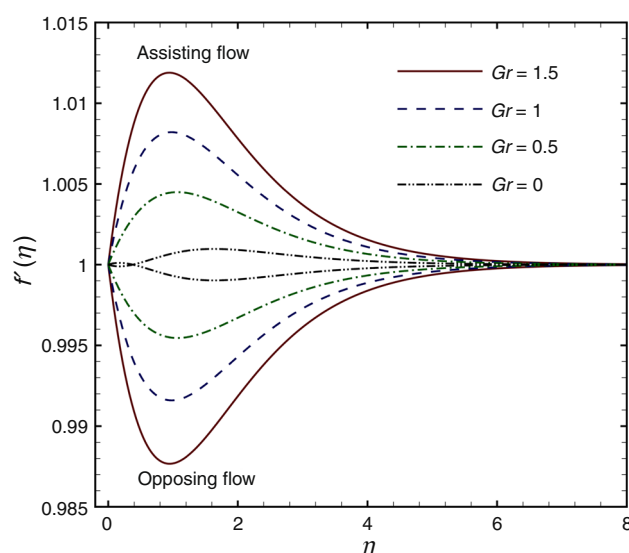


Fig. 8 Effects of Gr on velocity distribution

that the velocity of flow increases when buoyant forces increases, and an opposite behavior can be seen for opposing flow.

Variations of temperature profiles with different parameters are shown in Figs. 9–17. The effects of K and L on temperature profiles are presented in Figs. 9 and 10. Increase of either of the viscoelastic parameter or cross-viscous parameter has a result of increasing temperature and thermal boundary layer thickness. Here, the material parameter depends on normal stress and viscosity when K and L increase it means normal stresses increasing and viscous forces decreases. Same effects can be seen in Fig. 11 which depicts the influence of third-grade parameters. The impact of the cross-viscous parameter on

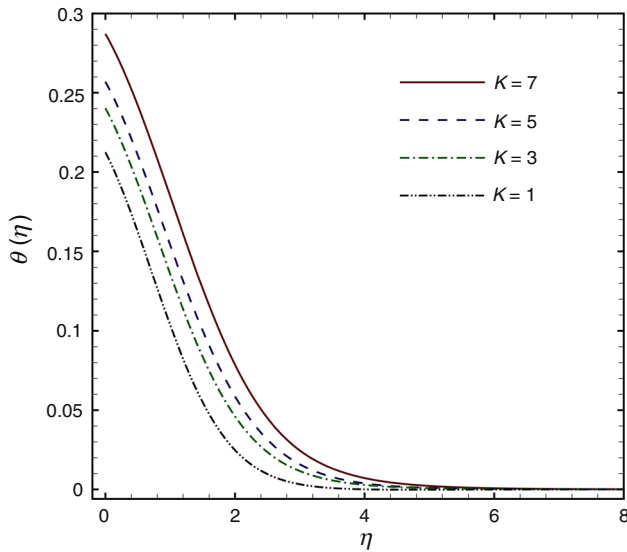


Fig. 9 Effects of K on temperature distribution with $c/a = 2$

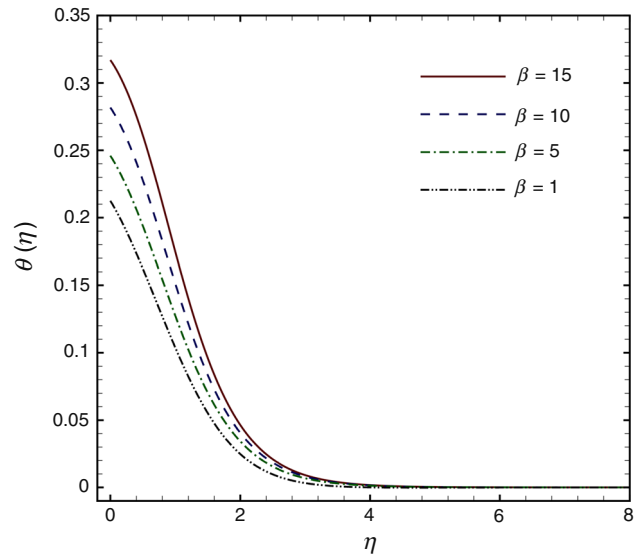


Fig. 11 Effects of β on temperature distribution when $c/a = 2$

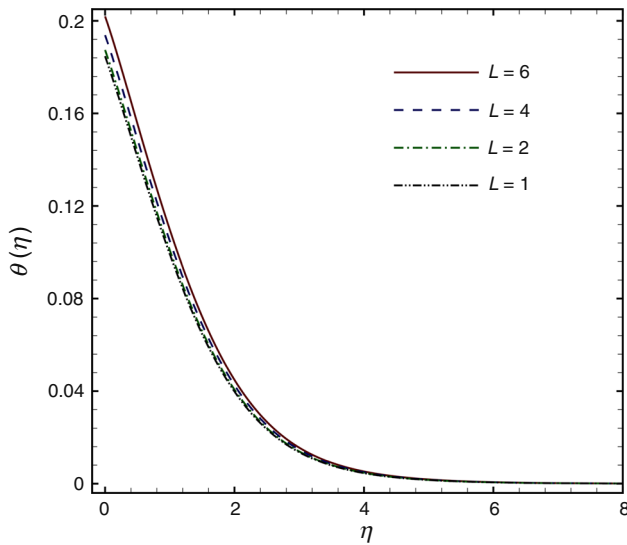


Fig. 10 Effects of L on temperature distribution with $c/a = 0.5$

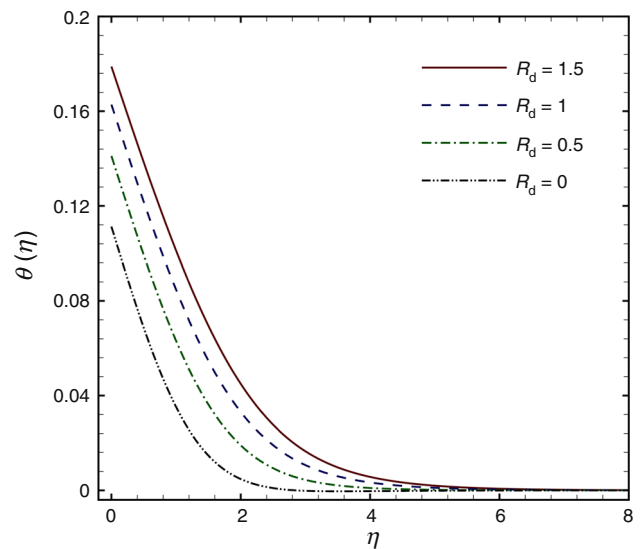


Fig. 12 Effects of R_d on temperature distribution

temperature is lesser than the viscoelastic and third-grade parameters. The impact of the radiation parameter on the temperature profiles is shown in Fig. 12. As expected, the temperature and thermal boundary layer thickness increase with an increase in radiation parameter. This is because the surface heat flux increases due to the effects of thermal radiation and as a result, larger temperature should be expected inside the boundary layer region.

Effects of magnetic field parameter on temperature are shown in Fig. 13. Increasing of temperature with increasing M is observed. This effect is because the fact that applying a magnetic field can create a Lorentz force which tends to retard the fluid motion and as a result temperature profiles increase as well as the thickness of the thermal

boundary layer. Therefore, temperature of the surface can be controlled by controlling the strength of the magnetic field. Opposite effect can be seen for Pr number in Fig. 14. With increasing Pr number, thermal diffusivity of the fluid decreases and as a result thermal boundary layer and temperature decrease. Variation of temperature profiles with Eckert number is presented in Fig. 15 which indicates that the increase of viscous dissipation or Ec number causes temperature rise in the boundary layer.

Increasing Bi parameter creates increment in temperature values. Bi is a ratio of the hot fluid side convection resistance to the cold fluid side convection resistance on a surface. If cold fluid properties and free stream velocity remain fixed, Bi is proportional to the heat transfer

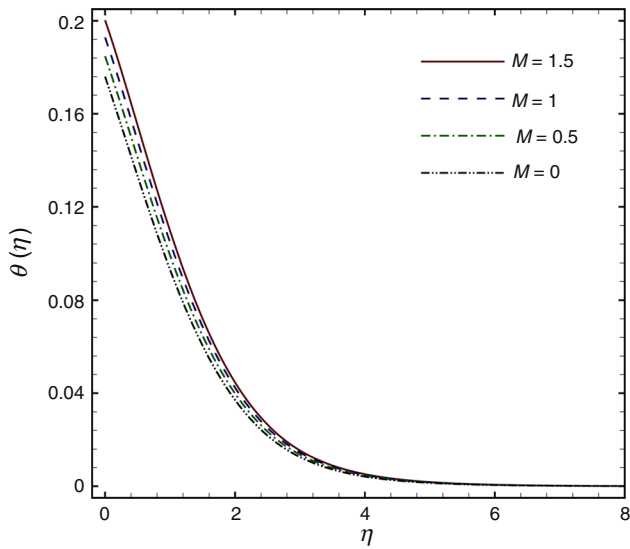


Fig. 13 Effects of M on temperature distribution when $c/a = 0.5$

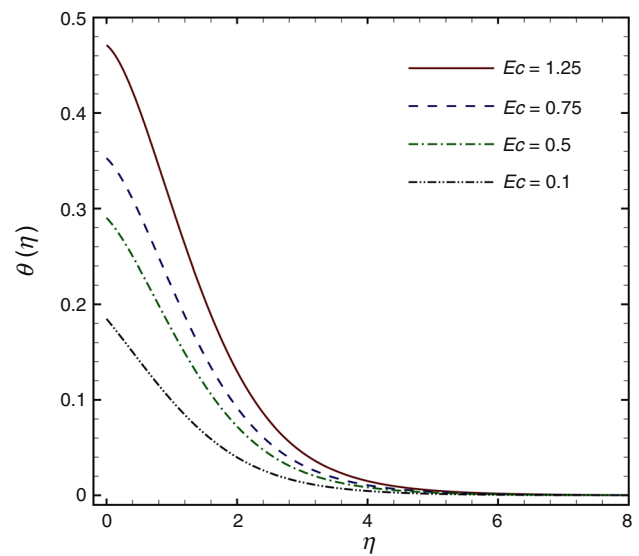


Fig. 15 Effects of Ec on temperature distribution when $c/a = 0.5$

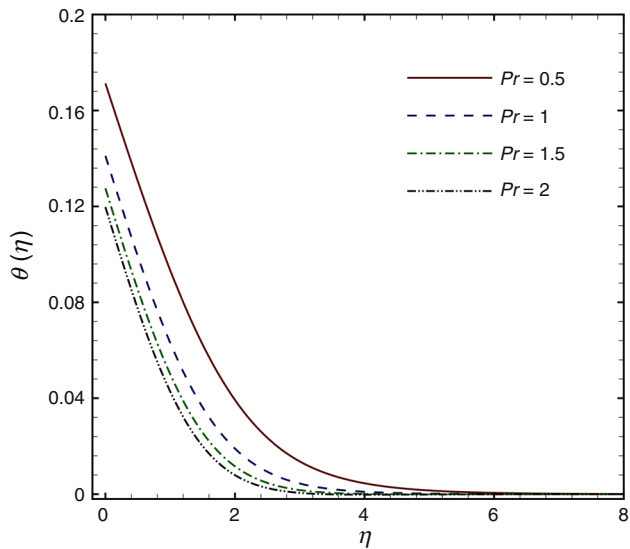


Fig. 14 Effects of Pr on temperature distribution

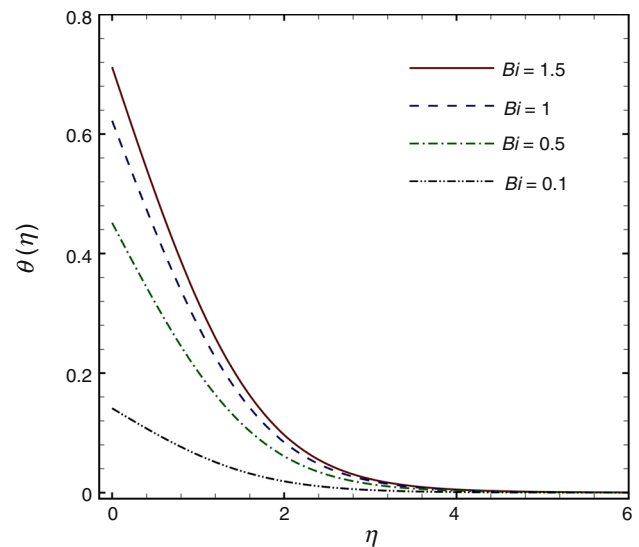


Fig. 16 Effects of Bi on temperature distribution

coefficient for the hot fluid. The thermal resistance is inversely proportional to heat transfer coefficient. Therefore, with increasing Bi , hot fluid side convection resistance decreases so the temperature and thermal boundary layer thickness increase (Fig. 16). From Fig. 17, it's obvious that Brownian motion parameter has very small influence on the temperature profiles. Same effect has been seen for thermophoresis parameter when $c/a = 1$; however, with increasing these parameters the temperature profiles and thermal boundary layer enhance slightly.

Effects of the non-dimensional parameters on the nanoparticle concentration profiles are shown in Figs. 18–25. It is shown in Fig. 18 that with larger values of cross-viscose parameter, when $c/a = 0.5$, the nanoparticle

concentration and their related thickness increase. It must be noted that for $c/a = 2$ an opposite behavior has been seen. Effect of third-grade parameter on concentration is sketched in Fig. 19. Higher values of the third-grade parameter tend to increase nanoparticle concentration and their related boundary thickness.

Figure 20 indicates the effects of the magnetic field parameter on ϕ . It can be seen that influence of M is similar to β but the nanoparticle concentration and its associated boundary thickness have more variations with β . Prandtl number has opposite impact on ϕ ; from Fig. 21, it can be seen that with larger values of Pr nanoparticle concentration and their related boundary thickness decreases. From Fig. 22, one can see that the profiles of concentration are

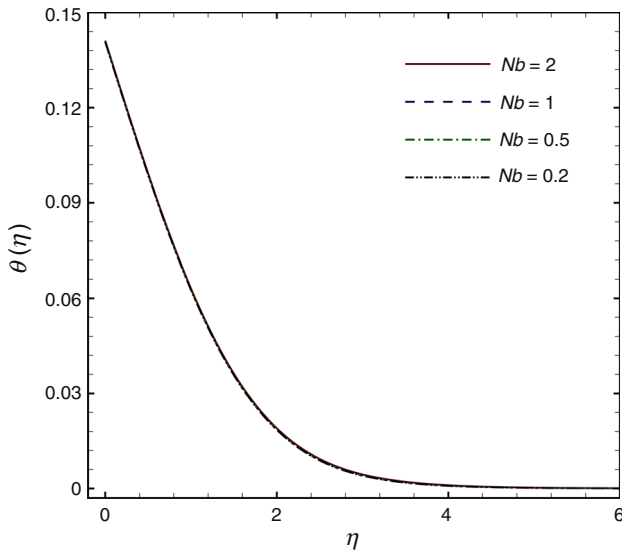


Fig. 17 Effects of Nb on temperature distribution

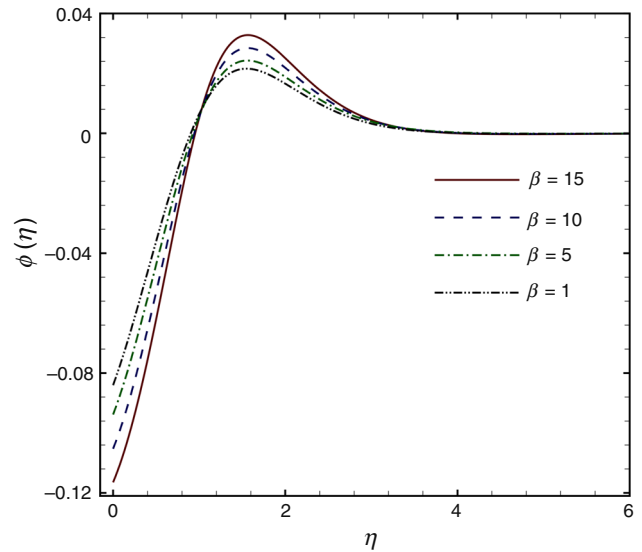


Fig. 19 Effects of β on nanoparticle concentration distribution when $c/a = 2$

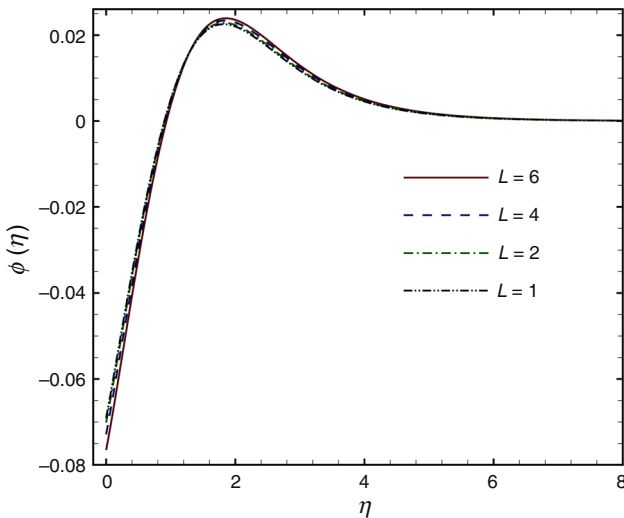


Fig. 18 Effects of L on nanoparticle concentration distribution when $c/a = 0.5$

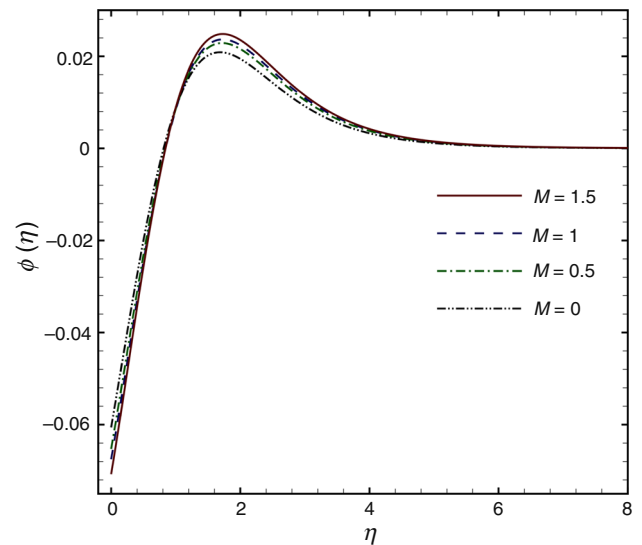


Fig. 20 Effects of M on nanoparticle concentration distribution when $c/a = 0.5$

higher for higher values of Bi and it causes larger boundary thickness for concentration.

The impact of Nt and Nb on ϕ is shown in Figs. 23 and 24, respectively. As it is shown in these figures, nanofluid parameters have opposite impacts on the concentration profiles, that is, with increasing thermophoresis parameter the nanoparticle concentration and their related boundary thickness increase but larger values of Brownian motion parameter tend to lower the ϕ values. Physically, increasing the thermophoresis parameter results in increment of thermophoresis force that means nanoparticles moving from hot to cold areas and as a result, magnitude of nanoparticle volume fraction increases. In addition, increasing Brownian motion parameter results in

decreasing the diffusion of nanoparticles into the fluid regime away from the surface, then ϕ decreases in the boundary layer. The nanoparticle concentration decreases when Le increases as shown in Fig. 25. For base fluid of certain thermal diffusivity (α), a higher Lewis number implies a lower Brownian diffusion coefficient which results in shorter penetration depth for the concentration boundary layer. Variation of nanoparticle concentration with Ec is presented in Fig. 26. It is seen that ϕ is an increasing function of Eckert number.

The numerical values of the local Nusselt number for different values of the velocity ratio and the other dimensionless parameters are shown in Table 2. As we

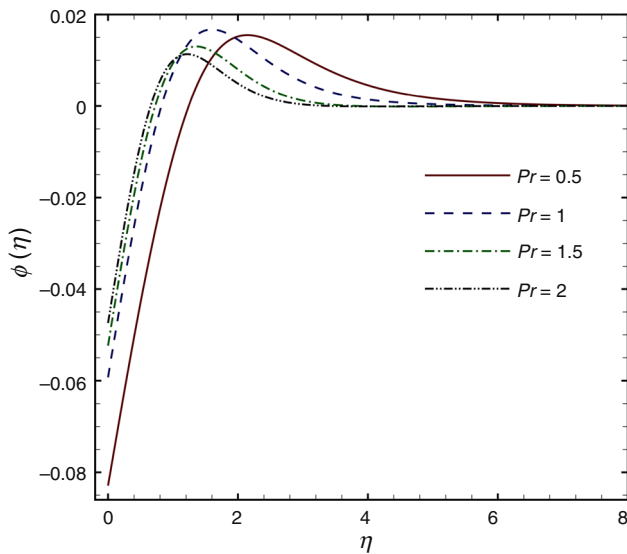


Fig. 21 Effects of Pr on nanoparticle concentration distribution

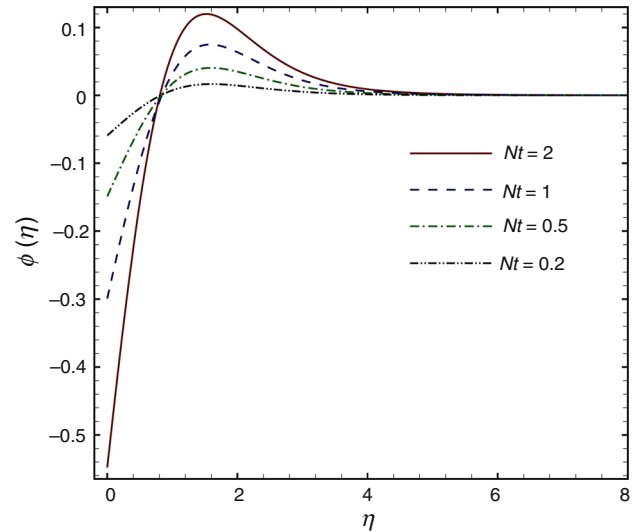


Fig. 23 Effects of Nt on nanoparticle concentration distribution

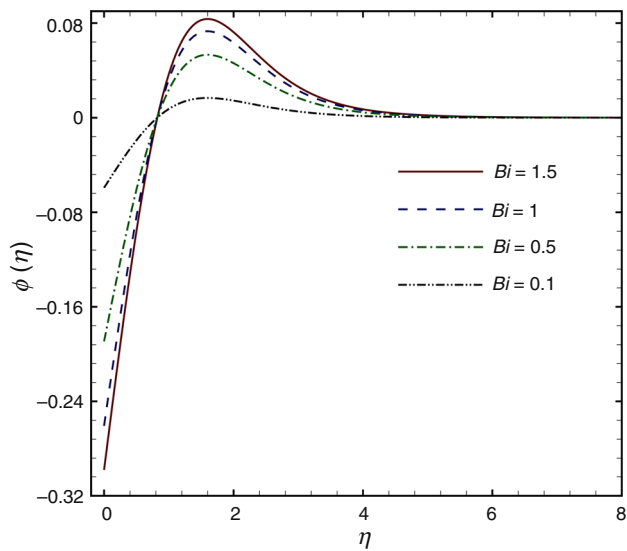


Fig. 22 Effects of Bi on nanoparticle concentration distribution

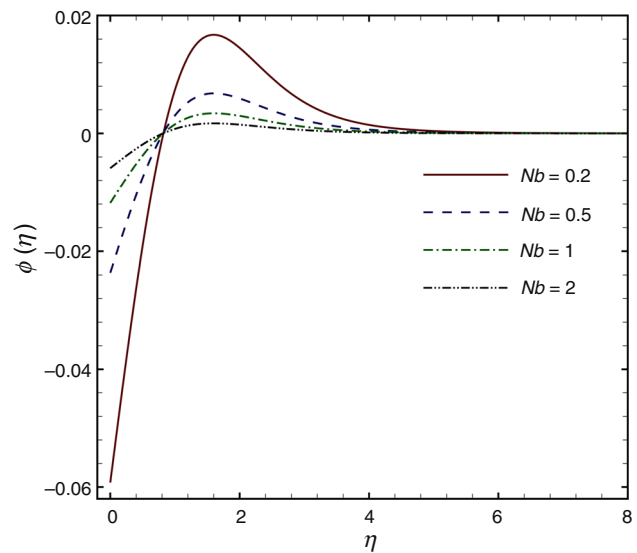


Fig. 24 Effects of Nb on nanoparticle concentration distribution

mentioned, for numerical solution another boundary condition is needed which is zero shear-stress at infinity. Also, we choose large enough value for η_∞ in computations. It's clear from Table 2 that when $c/a = 1$ the impact of $K, L, \beta, M, Ec, Nt,$ and Le is negligible also the influence of $Nb, Gr,$ and Br on local Nusselt number is very small for all the velocity ratios. Local Nusselt number increases when $Pr, Bi,$ and R_d increase and an opposite trend is noted for $K, Le,$

$Nt, Ec, M,$ and β . Another point is that cross-viscous parameters have opposite impact on local Nusselt number when $c/a > 1$ or $c/a < 1$.

Table 3 is shown to analyze values of the skin friction coefficient with different values of $K, \beta, L, M, Gr,$ and Br . The negative sign of $-C_f Re_x^{1/2}$ values, when $c/a = 0.5$, is due to the direction of the flow which is contrary to the x in this case.

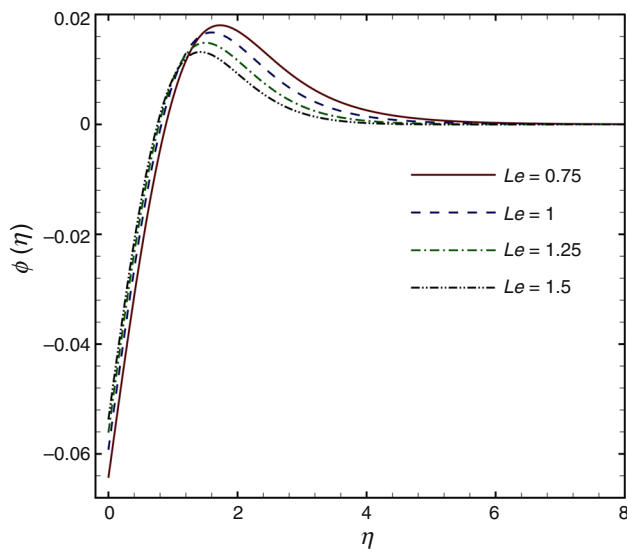


Fig. 25 Effects of L on nanoparticle concentration distribution when $c/a = 0.5$

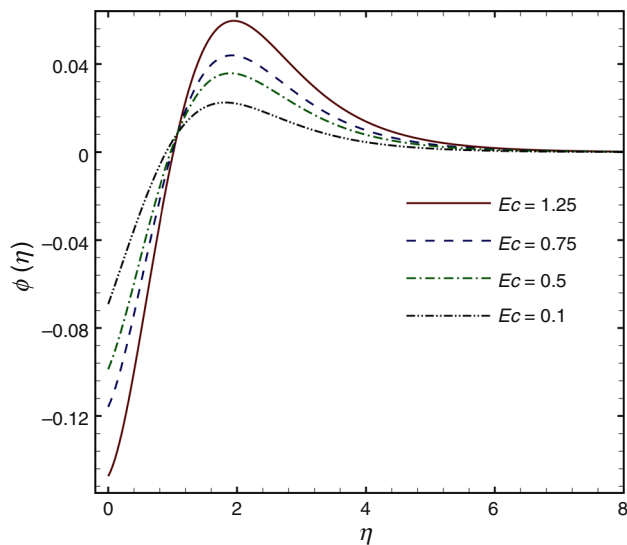


Fig. 26 Effects of Ec on nanoparticle concentration distribution when $c/a = 0.5$

Conclusions

In this paper, we have solved the problem of the mixed convection stagnation-point flow of a third-grade nanofluid over a vertical stretching sheet subjected to convective boundary condition. Analytical method named homotopy analysis method has been used to obtain the series solution of the problem. In this method, there is no need for an extra boundary condition to solve the equations of non-Newtonian fluid. The following results have been observed in this study:

- Viscoelastic parameter (K) and cross-viscous parameter (L) have the same impact on the velocity profiles and with an increase in either of the parameters the velocity profiles decrease. For temperature distribution, increasing either of the three parameters subjected to the third-grade fluid tends to increase temperature profiles. Same effects can be seen in nanoparticle concentration profiles.
- The dimensionless nanoparticle concentration and its related boundary layer increase with thermophoresis parameter and decrease with Brownian motion parameter. Also, thermophoresis parameter has low impact on the temperature distributions and an increase in Nt tends to decrease the local Nusselt number slightly, but the Brownian motions parameters impact is completely negligible.
- The temperature distribution enhances with increasing the Eckert number. Same effect can be seen for dimensionless nanoparticle concentration.
- Increasing magnetic field parameter (M) has impact of decreasing velocity profiles while opposite influence can be seen for the temperature and nanoparticle concentration profiles.

Table 2 Numerical values of the local Nusselt number for different non-dimensional parameters

<i>Pr</i>	<i>Le</i>	<i>Nb</i>	<i>Nt</i>	<i>Ec</i>	<i>Bi</i>	<i>M</i>	<i>R_d</i>	<i>Gr</i>	<i>Br</i>	β	<i>L</i>	<i>K</i>	$Nu_x Re_x^{-1/2}$		
													<i>c/a</i> = 0.5	<i>c/a</i> = 1	<i>c/a</i> = 2
1	1	0.2	0.2	0.1	0.1	0.5	0.5	0.5	0.5	1	1	1	0.13625	0.14343	0.13178
0.5	1	0.2	0.2	0.1	0.1	0.5	0.5	0.5	0.5	1	1	1	0.13118	0.13836	0.13039
1.5													0.13825	0.14556	0.13204
2													0.13932	0.14675	0.13208
1	0.75	0.2	0.2	0.1	0.1	0.5	0.5	0.5	0.5	1	1	1	0.13626	0.14344	0.13179
	1.25												0.13623	0.14343	0.13176
	1.5												0.13622	0.14342	0.13175
1	1	0.5	0.2	0.1	0.1	0.5	0.5	0.5	0.5	1	1	1	0.13622	0.14343	0.13177
		1											0.13621	0.14343	0.13177
		2											0.13620	0.14343	0.13177
1	1	0.2	0.5	0.1	0.1	0.5	0.5	0.5	0.5	1	1	1	0.13620	0.14337	0.13164
			1										0.13611	0.14327	0.13140
			2										0.13591	0.14306	0.13091
1	1	0.2	0.2	0.5	0.1	0.5	0.5	0.5	0.5	1	1	1	0.11906	0.14343	0.07290
				0.75									0.10887	0.14343	0.03461
				1.25									0.08960	0.14342	- 0.0462
1	1	0.2	0.2	0.1	0.5	0.5	0.5	0.5	0.5	1	1	1	0.42140	0.46011	0.43934
					1								0.57086	0.63516	0.61983
					1.5								0.64743	0.72730	0.71799
1	1	0.2	0.2	0.1	0.1	0.5	0.5	0.5	0.5	1	1	1	0.13777	0.14344	0.13535
						1							0.13488	0.14343	0.12841
						1.5							0.13362	0.14343	0.12521
1	1	0.2	0.2	0.1	0.1	0.5	0.5	0.5	0.5	1	1	1	0.08432	0.08885	0.07926
							1						0.18579	0.19583	0.18323
							1.5						0.23343	0.24650	0.23371
1	1	0.2	0.2	0.1	0.1	0.5	0.5	0	0.5	1	1	1	0.13595	0.14341	0.13190
								1					0.13651	0.14346	0.13165
								1.5					0.13676	0.14348	0.13152
1	1	0.2	0.2	0.1	0.1	0.5	0.5	0.5	0	1	1	1	0.13620	0.14343	0.13177
									1				0.13629	0.14344	0.13178
									1.5				0.13634	0.14344	0.13178
1	1	0.2	0.2	0.1	0.1	0.5	0.5	0.5	0.5	0	1	1	0.13632	0.14343	0.13344
										2			0.13619	0.14343	0.13052
										3			0.13616	0.14343	0.12950
1	1	0.2	0.2	0.1	0.1	0.5	0.5	0.5	0.5	1	0	1	0.13664	0.14343	0.13081
											2		0.13580	0.14343	0.13257
											3		0.13531	0.14343	0.13322
1	1	0.2	0.2	0.1	0.1	0.5	0.5	0.5	0.5	1	1	0	0.13581	0.14346	0.13625
												2	0.13620	0.14343	0.13099
												3	0.13605	0.14342	0.12922

Table 3 Numerical values of the skin friction coefficient for different non-dimensional parameters

K	β	L	M	Gr	Br	$-C_f Re_x^{1/2}$		
						$c/a = 0.5$	$c/a = 1$	$c/a = 2$
1	1	1	0.5	0.5	0.5	-4.315	0.0749	6.668
0	1	1	0.5	0.5	0.5	-2.187	0.0448	4.936
2						-5.773	0.0863	8.402
3						-6.947	0.0931	9.925
1	0	1	0.5	0.5	0.5	-4.326	0.0749	5.901
	2					-4.316	0.0749	7.242
	3					-4.322	0.0749	7.712
1	1	0	0.5	0.5	0.5	-3.886	0.0750	7.526
		2				-4.810	0.0748	5.959
		3				-5.377	0.0747	5.376
1	1	1	0	0.5	0.5	-3.823	0.0787	6.191
			1			-4.763	0.0716	7.127
			1.5			-5.175	0.0687	7.570
1	1	1	0.5	0	0.5	-4.529	-0.0128	6.568
				1		-4.119	0.1619	6.768
				1.5		-3.913	0.2479	6.869
1	1	1	0.5	0.5	0	-4.315	0.0879	6.691
					1	-4.316	0.0619	6.645
					1.5	-4.317	0.0489	6.622

Acknowledgements Financial support of Ferdowsi University of Mashhad under Contract No. 2/42929 is acknowledged.

References

- Sakiadis B. Boundary-layer behavior on continuous solid surfaces: I. Boundary-layer equations for two-dimensional and axisymmetric flow. *AIChE J.* 1961;7(1):26–8.
- Sakiadis B. Boundary-layer behavior on continuous solid surfaces: II. The boundary layer on a continuous flat surface. *AIChE J.* 1961;7(2):221–5.
- Erickson L, Fan L, Fox V. Heat and mass transfer on moving continuous flat plate with suction or injection. *Ind Eng Chem Fundam.* 1966;5(1):19–25.
- Ali M, Al-Yousef F. Laminar mixed convection from a continuously moving vertical surface with suction or injection. *Heat Mass Transf.* 1998;33(4):301–6.
- Chen C-H. Laminar mixed convection adjacent to vertical, continuously stretching sheets. *Heat Mass Transf.* 1998;33(5–6):471–6.
- Ali ME. The effect of variable viscosity on mixed convection heat transfer along a vertical moving surface. *Int J Therm Sci.* 2006;45(1):60–9.
- Ishak A, Nazar R, Pop I. Mixed convection boundary layers in the stagnation-point flow toward a stretching vertical sheet. *Meccanica.* 2006;41(5):509–18.
- Ishak A, Jafar K, Nazar R, Pop I. MHD stagnation point flow towards a stretching sheet. *Physica A.* 2009;388(17):3377–83.
- Hayat T, Abbas Z, Pop I, Asghar S. Effects of radiation and magnetic field on the mixed convection stagnation-point flow over a vertical stretching sheet in a porous medium. *Int J Heat Mass Transf.* 2010;53(1):466–74.
- Masuda H, Ebata A, Teramae K. Alteration of thermal conductivity and viscosity of liquid by dispersing ultra-fine particles. Dispersion of Al_2O_3 , SiO_2 and TiO_2 ultra-fine particles. *Netsu Bussei.* 1993;7(4):227–33.
- Chol S. Enhancing thermal conductivity of fluids with nanoparticles. *ASME Publ Fed.* 1995;231:99–106.
- Buongiorno J. Convective transport in nanofluids. *J Heat Transf.* 2006;128(3):240–50.
- Khan W, Pop I. Boundary-layer flow of a nanofluid past a stretching sheet. *Int J Heat Mass Transf.* 2010;53(11):2477–83.
- Haq RU, Nadeem S, Khan ZH, Akbar NS. Thermal radiation and slip effects on MHD stagnation point flow of nanofluid over a stretching sheet. *Physica E.* 2015;65:17–23.
- Makinde O, Aziz A. Boundary layer flow of a nanofluid past a stretching sheet with a convective boundary condition. *Int J Therm Sci.* 2011;50(7):1326–32.
- Aziz A. A similarity solution for laminar thermal boundary layer over a flat plate with a convective surface boundary condition. *Commun Nonlinear Sci Numer Simul.* 2009;14(4):1064–8.
- Mustafa M, Hayat T, Pop I, Asghar S, Obaidat S. Stagnation-point flow of a nanofluid towards a stretching sheet. *Int J Heat Mass Transf.* 2011;54(25):5588–94.
- Mabood F, Khan W. Analytical study for unsteady nanofluid MHD Flow impinging on heated stretching sheet. *J Mol Liq.* 2016;219:216–23.
- Makinde O, Khan W, Khan Z. Buoyancy effects on MHD stagnation point flow and heat transfer of a nanofluid past a convectively heated stretching/shrinking sheet. *Int J Heat Mass Transf.* 2013;62:526–33.

20. Malvandi A, Hedayati F, Ganji D. Slip effects on unsteady stagnation point flow of a nanofluid over a stretching sheet. *Powder Technol.* 2014;253:377–84.
21. Mansur S, Ishak A, Pop I. The magnetohydrodynamic stagnation point flow of a nanofluid over a stretching/shrinking sheet with suction. *PLoS ONE.* 2015;10(3):e0117733.
22. Rashid I, Haq RU, Al-Mdallal QM. Aligned magnetic field effects on water based metallic nanoparticles over a stretching sheet with PST and thermal radiation effects. *Physica E.* 2017;89:33–42.
23. Rahman M, Eltayeb I. Radiative heat transfer in a hydromagnetic nanofluid past a non-linear stretching surface with convective boundary condition. *Meccanica.* 2013;48(3):601–15.
24. Rana P, Dhanai R, Kumar L. Radiative nanofluid flow and heat transfer over a non-linear permeable sheet with slip conditions and variable magnetic field: dual solutions. *Ain Shams Eng J.* 2017;8(3):341–52. <https://doi.org/10.1016/j.asej.2015.08.016>.
25. Zaimi K, Ishak A, Pop I. Boundary layer flow and heat transfer over a nonlinearly permeable stretching/shrinking sheet in a nanofluid. *Sci Rep.* 2014;4:4404.
26. Malvandi A, Moshizi S, Ganji D. Nanoparticle transport effect on magnetohydrodynamic mixed convection of electrically conductive nanofluids in micro-annuli with temperature-dependent thermophysical properties. *Physica E.* 2017;88:35–49.
27. Rashidi S, Mahian O, Languri EM. Applications of nanofluids in condensing and evaporating systems. *J Therm Anal Calorim.* 2017;8:1–13.
28. Javadi P, Rashidi S, Abolfazli Esfahani J. flow and heat management around obstacle by nanofluid and incidence angle. *J Thermophys Heat Transf.* 2017;31(4):983–8.
29. Bovand M, Rashidi S, Esfahani J. Optimum interaction between magnetohydrodynamics and nanofluid for thermal and drag management. *J Thermophys Heat Transf.* 2016;31(1):218–29.
30. Shirejini SZ, Rashidi S, Esfahani J. Recovery of drop in heat transfer rate for a rotating system by nanofluids. *J Mol Liq.* 2016;220:961–9.
31. Akar S, Rashidi S, Esfahani JA. Second law of thermodynamic analysis for nanofluid turbulent flow around a rotating cylinder. *J Therm Anal Calorim.* 2018;2:1–12.
32. Dunn J, Rajagopal K. Fluids of differential type: critical review and thermodynamic analysis. *Int J Eng Sci.* 1995;33(5):689–729.
33. Fosdick R, Rajagopal K, editors. *Thermodynamics and stability of fluids of third grade.* In: *Proceedings of the royal society of London A: mathematical, physical and engineering sciences;* 1980. The Royal Society.
34. Rajagopal K, Szeri A, Troy W. An existence theorem for the flow of a non-Newtonian fluid past an infinite porous plate. *Int J Non Linear Mech.* 1986;21(4):279–89.
35. Maneschy C, Massoudi M, Ghoneimy A. Heat transfer analysis of a non-Newtonian fluid past a porous plate. *Int J Non Linear Mech.* 1993;28(2):131–43.
36. Sahoo B. Flow and heat transfer of an electrically conducting third grade fluid past an infinite plate with partial slip. *Meccanica.* 2010;45(3):319–30.
37. Sahoo B, Poncet S. Flow and heat transfer of a third grade fluid past an exponentially stretching sheet with partial slip boundary condition. *Int J Heat Mass Transf.* 2011;54(23):5010–9.
38. Shehzad S, Hussain T, Hayat T, Ramzan M, Alsaedi A. Boundary layer flow of third grade nanofluid with Newtonian heating and viscous dissipation. *J Cent South Univ.* 2015;22(1):360–7.
39. Hayat T, Aziz A, Muhammad T, Ahmad B. On magnetohydrodynamic flow of second grade nanofluid over a nonlinear stretching sheet. *J Magn Magn Mater.* 2016;408:99–106.
40. Hayat T, Aziz A, Muhammad T, Alsaedi A, Mustafa M. On magnetohydrodynamic flow of second grade nanofluid over a convectively heated nonlinear stretching surface. *Adv Powder Technol.* 2016;27(5):1992–2004.
41. Ghasemi SE, Hatami M, Sarokolaie AK, Ganji D. Study on blood flow containing nanoparticles through porous arteries in presence of magnetic field using analytical methods. *Physica E.* 2015;70:146–56.
42. Liao S. *Beyond perturbation: introduction to the homotopy analysis method.* Boca Raton: CRC Press; 2003.
43. Liao S. On the homotopy analysis method for nonlinear problems. *Appl Math Comput.* 2004;147(2):499–513.
44. Liao S-J. An approximate solution technique not depending on small parameters: a special example. *Int J Non Linear Mech.* 1995;30(3):371–80.
45. Liao S, Tan Y. A general approach to obtain series solutions of nonlinear differential equations. *Stud Appl Math.* 2007;119(4):297–354.
46. Kuznetsov A, Nield D. Natural convective boundary-layer flow of a nanofluid past a vertical plate: a revised model. *Int J Therm Sci.* 2014;77:126–9.
47. Rivlin RS, Ericksen J. *Stress-deformation relations for isotropic materials.* *Collected Papers of RS Rivlin.* Berlin: Springer; 1997. p. 911–1013.
48. Pakdemirli M. The boundary layer equations of third-grade fluids. *Int J Non Linear Mech.* 1992;27(5):785–93.